OXFORD

SOT | Society of Toxicology
academic.oup.com/toxsci

Tox Spotlight

Species-Specific Urothelial Toxicity With an Anti-HIV Noncatalytic Site Integrase Inhibitor (NCINI) Is Related to Unusual pH-Dependent Physicochemical Changes

Ruth A. Roberts [ID],[*,†,1] Richard A. Campbell,[‡] Phumzile Sikakana [ID],[*] Claire Sadler,[*] Mark Osier,[§,2] Yili Xu,[¶] Joy Y. Feng [ID],[¶] Michael Mitchell,[‖] Roman Sakowicz,[¶] Anne Chester,[§] Eric Paoli,[‖‖,3] Jianhong Wang,[**,4] and Leigh Ann Burns-Naas[§,5]

[*]ApconiX, Alderley Park, SK10 4TG, UK; [†]University of Birmingham, B15 2TT, UK; [‡]Division of Pharmacy and Optometry, University of Manchester, Manchester M13 9PT, UK; [§]Nonclinical Safety & Pathobiology, Gilead Sciences, Inc., Foster City, California 94404, USA; [¶]Biology, Gilead Sciences, Inc., Foster City, California 94404, USA; [‖]Medicinal Chemistry, Gilead Sciences, Inc., Foster City, California 94404, USA; [‖‖]Formulations and Process Development, Gilead Sciences, Inc., Foster City, California 94404, USA; and [**]Drug Metabolism & Pharmacokinetics, Gilead Sciences, Inc., Foster City, California 94404, USA

[2]Present address: Pliant Therapeutics, South San Francisco, CA 94080, USA

[3]Present address: Verily Life Sciences, South San Francisco, CA 94080, USA

[4]Present address: Cortexyme, Inc., South San Francisco, CA 94080, USA

[5]Present address: Magnolia Toxicology Consulting, LLC, Traverse City, MI 49683, USA

[1]To whom correspondence should be addressed. E-mail: ruth.roberts@apconix.com.

ABSTRACT

GS-9695 and GS-9822 are next-generation noncatalytic site integrase inhibitors (NCINIs) with significantly improved potency against human immunodeficiency virus compared with previous drugs such as BI-224436. Development stopped due to vacuolation of the bladder urothelium seen in cynomolgus monkey but not in rat; this lesion was absent in equivalent preclinical studies with BI-224436 (tested in dog and rat). Lesions were unlikely to be attributable to target because NCINIs specifically target viral integrase protein and no mammalian homologue is known. Secondary pharmacology studies, mitochondrial toxicity studies, immunophenotyping, and analysis of proteins implicated in cell-cell interactions and/or bladder integrity (E-cadherin, pan-cytokeratin, uroplakins) failed to offer any plausible explanation for the species specificity of the lesion. Because it was characterized by inflammation and disruption of urothelial morphology, we investigated physicochemical changes in the bladder of cynomolgus monkey (urinary pH 5.5–7.4) that might not occur in the bladder of rats (urinary pH 7.3–8.5). In measurements of surface activity, GS-9822 showed an unusual transition from a monolayer to a bilayer at the air/water interface with decreasing pH, attributed to the strong association between drug molecules in adjacent bilayer leaflets and expected to be highly disruptive to the urothelium. Structural analysis of GS-9822 and GS-9695 showed zwitterionic characteristics over the range of pH expected in cynomolgus monkey but not rat urine. This exotic surface behavior is unlikely with BI-224436 since it would transition from neutral to cationic (never zwitterionic)

with decreasing pH. These data provide useful insights to guide discovery and development of NCINIs, related compounds, and zwitterions.

Key words: bladder; HIV; NCINI; urothelial toxicity; mitochondrial toxicity; zwitterions.

Significant advances in the treatment and prophylaxis of human immunodeficiency virus (HIV)-1, coupled with widespread education programs, have reduced the number of new infections over the past decade. However, resistance to existing antiviral agents remains a challenge and provides a compelling need for the continued development of new therapeutic drug classes. One of the classes of approved antiretroviral drugs is the HIV integrase inhibitors. HIV integrase catalyzes strand transfer reactions during integration of the viral DNA into the host genome (Pommier et al., 2005). These drugs are also referred to as integrase (IN) strand (S) transfer (T) inhibitors (I) or INSTIs. The viral integrase enzyme comprises 3 domains: N-terminal, catalytic core, and C-terminal, and currently approved INSTIs target the catalytic core.

Dimerization of the catalytic core produces a cleft which serves as an allosteric binding site for the host protein lens-epithelium-derived growth factor (LEDGF)/transcriptional coactivator p75 (reviewed in Engelman and Cherepanov, 2008; Poeschla, 2008). Disruption of the LEDGF/p75-binding site reduces integration efficiency and growth of clinical viral isolates is blocked completely in somatic knock-out models (Llano et al., 2006; Marshall et al., 2007; Schrijvers et al., 2012; Shun et al., 2007; Vandekerckhove et al., 2006). Allosteric inhibitors of integrase therefore represent a new class of antiviral drugs known as the noncatalytic integrase inhibitors, or next-generation noncatalytic site integrase inhibitors (NCINIs), with potential activity against viruses harboring INSTI resistance mutations. Furthermore, recent studies indicate that NCINIs can have a dual action by blocking the interaction between integrase and LEDGF and by inhibiting integrase enzymatic activity (Kessl et al., 2012; Tsiang et al., 2012). The binding of NCINIs to the integrase dimer interface promotes integrase multimerization and disruption of proper core maturation which renders the progeny virus noninfectious (Jurado et al., 2013; Mitchell et al., 2017). With this new understanding of the antiviral effects of NCINIs and the continuing need for new antiviral mechanisms to treat HIV, there is increased interest in further optimization and subsequent clinical development of these compounds as a novel class of antiretrovirals with a unique, orthogonal mechanism of action. One of the first NCINIs to enter the clinic was BI-224436 (Fader et al., 2014).

GS-9695 and GS-9822 are next-generation NCINIs with significantly improved potency compared with BI-224436 (Mitchell et al., 2017) (see Figure 1 for the 3 structures). Although designed around the same key pharmacophore and benzothiazole core, GS-9822 is structurally distinct from GS-9695, possesses a much-improved resistance profile compared with GS-9695 and has a significantly higher resistance barrier than the approved, second-generation, reverse-transcriptase inhibitor rilpivirine (Mitchell et al., 2017). Based on these favorable parameters and the high selectivity index based on cellular toxicity (data not shown), GS-9695 progressed into early toxicology testing. However, following unusual toxicity results with GS-9695, GS-9822 also entered early toxicology testing.

GS-9695 and GS-9822 had no mutagenic activity (Ames mutagenicity test), no significant risk of clinical QT prolongation (as determined by in vitro hERG channel profiling) and had favorable secondary pharmacology profiles that supported clinical progression, with only minor activity (>50% inhibition at $10 \mu M$) at a few receptors: the only common receptor affected by both compounds being the glucocorticoid receptor, an unlikely candidate for the toxicity observed in vivo.

Preliminary in vivo toxicology studies were performed in both rats (Wistar Han) and cynomolgus monkeys to support first-in-human clinical studies. No adverse effects were identified following dosing of GS-9695 in rats at exposures approximately 15-fold greater than the estimated clinically efficacious exposure (see Supplementary Table 1 and footnote). Similar exposures to GS-9822 in rats resulted in toxicity based on decreased body weight and changes in clinical pathology parameters indicative of hepatocellular and hepatobiliary injury or interference with bilirubin transport (see Supplementary Table 2), though there was no histologic evidence observed in the liver. The development of both GS-9695 and GS-9822 was suspended, however, following a finding of reproducible urothelial toxicity that arose in cynomolgus monkeys after only 7 days of oral dosing. In this article, we describe these findings and the investigations conducted to understand their origin. As might be expected for an investigative drug safety program conducted over almost a decade, involving multiple contract laboratories and limited test material, the data are incomplete with some gaps and inconsistencies that would be challenging to correct, principally for ethical (animal welfare) reasons. However, the results provide useful insights to guide the development of NCINIs and related compounds, and others with zwitterionic characteristics.

MATERIALS AND METHODS

Test articles. GS-9695, GS-9822, and BI-224436 were prepared by Gilead Sciences, Foster City, California.

Animal welfare statement. All animal studies were conducted in laboratories fully accredited by the Association for Assessment and Accreditation of Laboratory Animal Care. All procedures were in compliance with applicable animal welfare acts and were approved by the local Institutional Animal Care and Use Committee.

Fourteen-day toxicology studies in rats. Test article was administered orally to 7–8 week-old Wistar Han rats ($n = 5$/sex/group) on 14 consecutive days at 0 (vehicle), 30, 100, or 300 mg/kg/day of GS-9695 or, 0 (vehicle), 20, 60, or 200 mg/kg/day of GS-9822. The vehicle controls for GS-9695 and GS-9822 groups were 0.5% (w/v) hydroxypropyl methylcellulose (HPMC), 0.1% (v/v) Tween 20, and 0.9% (v/v) benzyl alcohol in reverse osmosis (RO) water, and 0.5% HPMC, 0.1% Tween 20. Assessment of toxicity was based on mortality, clinical observations, food consumption, body weight, body weight change, and clinical and anatomic pathology. Blood samples were collected for toxicokinetic evaluations. For GS-9822, the in-life portion and necropsy were conducted by WIL Research, Ashland, Ohio and slides were prepared and assessed by Experimental Pathology Laboratories, Inc. (EPL), Virginia. For GS-9695, the in-life portion, necropsy, and
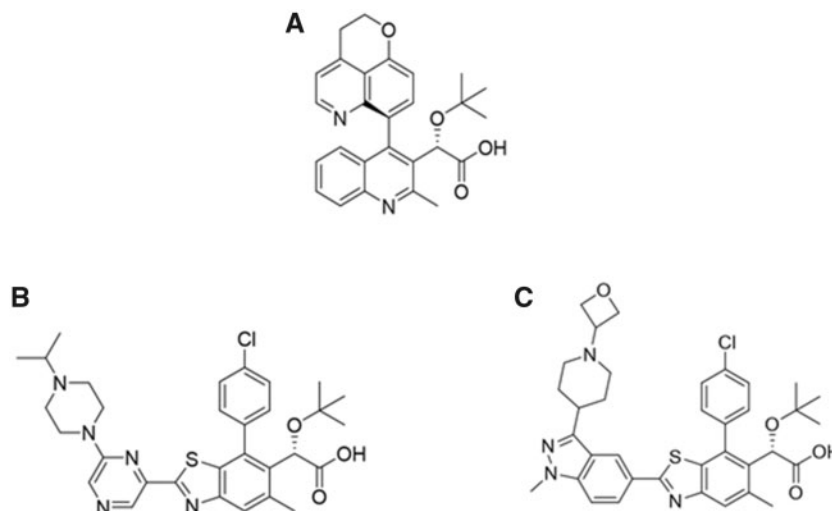
Figure 1. Structures of noncatalytic integrase inhibitors (NCINIs): A, BI-224436 (MW = 442.5), B, GS-9695 (MW = 594.2), C, GS-9822 (MW = 659.2). GS-9695 and GS-9822 are zwitterions with pK_a values of 4 and 7.8 (GS-9695) and 4.2 and 5.8 (GS-9822), respectively. Note the piperidine group attached to an oxetane group has a pK_a of approximately 6–7 (Wuitschik *et al.* 2006, 2010), whereas the carboxylic acid group has a pK_a approximately 4–5 (Smith and March, 2006). Molecular weight (MW).

pathological analysis were conducted by Covance Labs, Madison, Wisconsin.

Seven-day toxicology studies in cynomolgus monkeys. Test article was administered orally to cynomolgus monkeys ($n = 3$/sex/group) on 7 consecutive days at 0 (vehicle), 20, 60, or 300 mg/kg/day (GS-9695) or, 0 (vehicle), 20, 60, or 200 mg/kg/day (GS-9822) in a vehicle of 0.5% HPMC (w/v), 0.1% (v/v) Tween 20, and 0.9% (v/v) benzyl alcohol in RO water. Assessment of toxicity was based on mortality, clinical observations, food consumption, body weight, body weight change, and clinical and anatomic pathology. Blood samples were collected for toxicokinetic evaluations. For GS-9695, the in-life portion, necropsy, and pathological analyses were conducted by Covance Labs, Madison, Wisconsin. For GS-9822, the in-life portion and necropsy were conducted by WIL Research, Ashland, Ohio and slides were prepared and assessed by light microscopy at EPL, Virginia.

Transmission electron microscopy. At necropsy, following 7 days of oral dosing with either GS-9695 or GS-9822, trimmed sections of the urinary bladder (including the dome, mid, and trigone regions) were collected and placed into half strength Karnovsky's (GS-9695) or McDowell-Trump's 4F:1G (GS-9822) fixative. Sections were embedded in epoxy resin blocks, sectioned at 1 μm, stained with toluidine blue, and examined by light microscopy to identify areas of interest. Blocks were trimmed, and thin sections were taken, placed onto grids, and stained. Grids were examined by electron microscopy, and representative images were collected. Transmission electron microscopy (TEM) was performed at Covance (GS-9695) or the Laboratory for Neurotoxicity Studies, Virginia-Maryland College of Veterinary Medicine, Virginia Tech, Blacksburg (GS-9822).

Secondary pharmacology. The activities of GS-9695 and GS-9822 were assessed in a Lead Profiling Screen (74 targets) using radioligand-binding assays (Eurofins Panlabs, Taiwan). IC_{50} values were calculated by a nonlinear, least squares regression analysis and significant responses (>50% inhibition/stimulation) were noted.

Mitochondrial toxicity. Mitochondrial toxicity was assessed by measuring the oxygen consumption rate (OCR) of mitochondrial respiration using the Agilent Seahorse XF Cell Mito Stress Test using published protocols (Dranka *et al.,* 2011; Feng *et al.,* 2016). Human prostate cancer (PC-3) cells were treated with GS-9695, GS-9822, or BI-224436 over a range of concentrations for 4 h (GS-9695, GS-9822), 24 h (GS-9695, GS-9822, BI-224436), or 72 h (GS-9695, BI-224436). The OCR signals, normalized by cell numbers using DNA content and parallel experiments to measure ATP levels, were all based on the published protocol (Feng *et al.,* 2016). Rotenone, antimycin A, phenformin, and chloramphenicol were used as positive controls to show specific inhibition of mitochondrial respiration. Ionomycin was used as a negative control to show nonspecific inhibition of mitochondrial respiration. PC-3 cells were chosen for use in the Seahorse assay because they had previously been shown to be the most sensitive of 15 tested cell lines to the known mitochondrial effects of the nucleoside/nucleotide class of antiretroviral agents (data not shown). The 72 h timepoint had been previously shown as necessary to observe delayed mitochondrial toxicity such as that associated with nucleoside/nucleotides (data not shown). Data analysis and calculation of the concentration required to reach 20% and 50% effects were performed according to the published protocol (Feng *et al.,* 2016).

The effect of compounds on electron transport chain (ETC) complexes was measured by Mitologics SAS (Paris, France). Liver mitochondria from 6-week-old BALB/c female mice (Charles River, Saint-Germain-sur-L'arbresle, France) were isolated and purified by isopycnic density-gradient centrifugation in Percoll, as described previously (Buron *et al.,* 2010; Lecoeur *et al.,* 2004). Measurement of ETC complex enzymatic activities were conducted following published protocols (Benit *et al.,* 2006; Rustin *et al.,* 1994).

Urinary concentration evaluation. Six male Wistar Han rats or 5 female cynomolgus monkeys were dosed orally with 300 mg/kg/day GS-9695 for 7 consecutive days. Urine samples were collected 0–12 h and 12–24 h following dose administration from all animals on the first and last day of the study. For rats, samples were collected on ice into a specimen container using plastic bottomed metabolism cages. For cynomolgus monkeys, urine

was collected on wet ice using cage pans. At the end of the study, animals were returned to the stock colony.

Exploratory immunology and post-mortem artifact investigation. GS-9695 was administered orally to female cynomolgus monkeys at dose levels of 0 (vehicle; $n = 1$) or 300 mg/kg/day ($n = 2$) for 7 consecutive days at a volume of 5 ml/kg. Assessment of toxicity was based on mortality, clinical observations, body weights, and anatomic pathology (including immunohistochemistry). Assessment of potential immunomodulatory effects were based on *in vitro* evaluation in samples obtained prior to dosing, peripheral blood immunophenotyping of the monocyte population, and clinical pathology comparing predose and end of dosing samples. Immunophenotyping samples were stained on the same day as collection and evaluated for the following monocyte subsets: CD14+/CD16−/CD69−; CD14+/CD16+/CD69−; CD14+/CD16−/CD69+; and CD14+/CD16+/CD69+. Immunophenotyping results were enumerated as percent relative (%) and absolute (cells/µl) values for each phenotype, along with the absolute (cells/µl) monocyte values. An additional investigation was performed *in vitro* on blood collected predose (2 weeks or immediately prior to dosing) and at termination. Predose samples were cultured in the presence of GS-9695 (at 15, 30, or 70 µg/ml) ± lipopolysaccharide (LPS) for 1 h at 37°C prior to evaluation by flow cytometry.

At study termination, anatomic samples of 3 regions of the bladder (dome, mid, and trigone), ureter and kidney were sampled either immediately after euthanasia, or were allowed to sit for 30 min prior to fixation. These data eliminated the possibility that the observations in the original studies were due to artefact.

Immunohistochemistry: E-cadherin and pan-cytokeratin. Paraffin-embedded blocks containing urinary bladder from the cynomolgus monkeys treated with GS-9695 or GS-9822 in the 7-day repeat dose toxicity studies described above were shipped under ambient conditions via overnight courier to EPL, Durham, North Carolina. Two 4–6 µm sections were microtomed onto adhesive glass slides from all males in the GS-9822 high dose group (200 m/kg/day) and all males in the corresponding control group, and from all males and females in the GS-9695 high-dose group (300 mg/kg/day) and the corresponding control group. One slide was stained with E-cadherin, the other was stained with pan-cytokeratin. All available immunohistochemical sections were evaluated by the study pathologist via light microscopy at EPL, Durham, North Carolina.

Immunohistochemistry: Uroplakin. As a result of the earlier immunohistochemistry and electron microscopy evaluations, there were no cynomolgus tissues remaining from the previous repeat dose studies with GS-9695 or GS-9822. Thus, paraffin-embedded blocks containing kidney from naïve rat or cynomolgus monkey were obtained and shipped to Histologix, Nottingham, UK. Bladder tissue could not be obtained commercially so kidney tissue was selected for study due to the continuity of the urothelium between the bladder and ureters. Sections were microtomed onto glass slides in preparation for staining. Paraformaldehyde, neutral buffered formalin, and acetone fixatives were compared; paraformaldehyde showed a marginally stronger signal so was used for final slides. UPK3BL, a polyclonal antibody against Uroplakin IIIb-like protein, was titrated (1:20–1:160) to find the optimal concentration of 1:20 which was used for staining. Negative controls omitted the primary antibody. Sections were evaluated by light microscopy.

Surface activity measurements. The surface activity of GS-9822 was characterized by measurements of the surface pressure and ellipsometric phase shift, *d*(delta), with time at the air/water interface at pH 3, 5, and 7. A drug concentration of 20 µM was chosen based on the mean concentration of drug observed in cynomolgus monkey urine *in vivo* (16.97 nM at day 7; see Results section and Table 3). The solutions were made with 0.1 M NaCl (Sigma; >99.5%) and 0.1 M KCl (Fluka; analytical grade) in ultrapure water (Suez Select Fusion; resistivity 18.2 MΩ.cm) in order to mimic typical salt concentrations in urine (Park *et al.*, 2016). The pH was adjusted using HCl (Sigma Aldrich; ACS reagent). Note that due to the insolubility of GS-9695 at pH 3, 5, and 7, surface activity measurements could not be conducted (Supplementary Figure 5).

Measurements of surface activity were performed in duplicate by pouring 50 ml of fresh drug solution into an 8-cm PTFE dish. Each sample was thoroughly aspirated to clean the air/water interface immediately prior to the start of the measurement. This process was performed to remove any kinetically trapped drug (where present) and set the zero time of adsorption for kinetic comparisons (Tummino *et al.*, 2018).

Values of the surface pressure were measured using an alloy Wilhelmy plate using a G2 instrument (Kibron, Finland). The surface pressure equals the difference in surface tension between a sample and pure water, and the surface tension is calculated from the force exerted on the plate by the liquid. Although various factors can affect the kinetics of adsorption, the equilibrium surface pressure can be thought of as the ability of a drug to lower the surface tension of the air/water interface due to adsorption, that is, its surface activity. Uncertainty in the calibration is estimated as ± 1 mN/m (millinewton/meter).

Values of *d*(delta) were measured using an EP4 instrument (Accurion, Germany) at a wavelength of 489 nm and an angle of incidence of 50˚. Ellipsometry is a laser reflection technique where at the air/water interface *d*(delta) is the change in phase of light related to the amount (and ordering) of species in the layer (de Feijter *et al.*, 1978). Quantitative modeling of *d*(delta) to the adsorbed amount is straightforward for systems where no preferred orientations are exhibited (Angus-Smyth *et al.*, 2012) but can be complicated if there is strong orientational ordering of the adsorbed species (Ducharme *et al.*, 1990). As such, data are presented simply as values of *d*(delta) for qualitative comparison from system to system.

RESULTS

General Toxicology Findings in Rats and Nonhuman Primates
Standard toxicology tests and pharmacokinetic characterization of GS-9695 and GS-9822 were performed in Wistar Han rats (Supplementary Tables 1 and 2). Signs of systemic toxicity were only observed at the high dose reflecting a 12- to 15-fold exposure margin to the projected clinically efficacious exposure. The NOAEL for these compounds was defined based on lack of adversity (GS-9695 NOAEL = 300 mg/kg/day) or on mortality (GS-9822 NOAEL = 60 mg/kg/day). No bladder lesions were observed in rats with either compound at any of the doses, including supraclinical exposure levels.

Standard toxicology tests and pharmacokinetic characterization of GS-9695 and GS-9822 were performed in cynomolgus monkeys (Table 1, expanded in Supplementary Tables 3 and 4). In the 7-day toxicity study with GS-9695, urothelial lesions occurred in 2/6 animals at 20 mg/kg/day, increasing to 5/6 and 6/6 animals at 60 and 300 mg/kg/day, respectively. At all doses,

Table 1. Incidence and Severity of Histological Observations in the Renal Tract of Cynomolgus Monkeys Treated for 7 Days With Either GS-9695 or GS-9822

Tissue/finding	Sex	Male				Female			
GS-9695 Dose (mg/kg/day)		0	20	60	300	0	20	60	300
Urinary Bladder	No. examined:	3	3	3	3	3	3	3	3
Vacuolation, urothelium									
Total number affected		0	1	3	3	0	1	2	3
Minimal		0	1	1	0	0	1	0	0
Slight		0	0	1	2	0	0	1	1
Moderate		0	0	1	0	0	0	1	2
Marked		0	0	0	1	0	0	0	0
Hemorrhage									
Total number affected		0	0	1	1	0	0	0	2
Minimal		0	0	1	1	0	0	0	1
Slight		0	0	0	0	0	0	0	1
Inflammation									
Total number affected		0	0	0	3	0	0	1	3
Minimal		0	0	0	1	0	0	0	0
Slight		0	0	0	0	0	0	0	0
Moderate		0	0	0	2	0	0	1	2
Kidney	No. examined:	3	3	3	3	3	3	3	3
Vacuolation, urothelium									
Total number affected		0	0	1	3	0	0	2	2
Minimal		0	0	0	1	0	0	1	1
Slight		0	0	1	0	0	0	1	1
Moderate		0	0	0	2	0	0	0	0
Inflammation, pelvis									
Total number affected		0	0	1	2	0	0	0	1
Minimal		0	0	0	0	0	0	0	0
Slight		0	0	1	1	0	0	0	1
Moderate		0	0	0	1	0	0	0	0
Ureter	No. examined:	3	3	3	3	3	3	3	3
Vacuolation, urothelium									
Total number affected		0	0	0	2	0	0	0	1
Minimal		0	0	0	0	0	0	0	1
Slight		0	0	0	2	0	0	0	0
Inflammation									
Total number affected		0	0	0	2	0	0	0	1
Minimal		0	0	0	1	0	0	0	1
Slight		0	0	0	1	0	0	0	0
GS-9822 Dose (mg/kg/day)		0	20	60	200				
Urinary Bladder	No. examined:	3	3	3	3				
Vacuolation, urothelium									
Total number affected		0	0	1	2				
Minimal		0	0	1	1				
Slight		0	0	0	1				
Hemorrhage, submucosa									
Total number affected		0	0	0	1				
Minimal		0	0	0	1				
Inflammation, mixed cell, submucosa									
Total number affected		0	0	1	3				
Minimal		0	0	1	2				
Slight		0	0	0	1				
Kidney	No. examined:	3	3	3	3				
Vacuolation, urothelium									
Total number affected		0	0	0	2				
Minimal		0	0	0	0				
Slight		0	0	0	2				
Ureter	No. examined:	3	3	3	3				
Vacuolation, urothelium									
Total number affected		0	0	0	2				
Minimal		0	0	0	1				
Slight		0	0	0	1				

transitional cell vacuolation of the bladder urothelium was observed whereas involvement of the kidney was noted at 60 and 300 mg/kg/day and lesions in the ureter were reported at 300 mg/kg/day (Table 1). GS-9822 was also associated with urothelial toxicity in cynomolgus monkeys with a similar dose-dependent trend to that seen with GS-9695: at 60 mg/kg/day 1/3 animals had evidence of transitional cell vacuolation in the bladder urothelium, rising to 2/3 animals at the 200 mg/kg/day dose (Table 1). As with GS-9695, increasing exposure to GS-9822 also led to increasing involvement of the upper urinary tract, including inflammation and/or hemorrhage, in a larger proportion of animals (Table 1).

Light and Transmission Electron Microscopy in Cynomolgus Monkey
Representative histopathology and TEM sections of cynomolgus monkey urothelium with and without exposure to GS-9695 or GS-9822 are shown in Figures 2 and 3.

For both GS-9695 and GS-9822, vacuolation was present in the urothelium of 1 or more segments of the urinary tract (Table 1). The vacuolation, which was most severe in the urinary bladder (Figure 2), was noted primarily in the intermediate and superficial (umbrella cells) layers and was often characterized by an apparent separation of the superficial urothelial cells from underlying intermediate cell layer resulting in bullous formation. No evidence of widespread degeneration/necrosis or hyperplasia was present. Also in the urinary bladder, inflammation was often associated with vacuolation and comprised a mixed cellular response that reflected a more active process (compared with incidental mononuclear infiltrates also noted). Hemorrhage occurred less frequently and was generally associated with inflammation.

Special stains for the detection of macrophage markers CD68 and CD163 showed no evidence of a distinctive macrophage infiltrate into the mucosal/submucosal regions or any distinctive macrophage association with vacuolation in the urinary bladder, ureter, or kidney (pelvis) urothelium (data not shown). Immunolabeling staining for CD68 and CD163 was variable, with frequent positive labeling of urothelial cells and interstitial fibroblasts in control and dosed animals (data not shown).

For both GS-9695 and GS-9822, drug-related ultrastructural findings correlating with the light microscopic finding of transitional cell (urothelium) vacuolation included the striking feature of the loosening of intercellular attachments (intercellular adhesion), primarily in the superficial to intermediate urothelium, and resulted in increased intercellular clear space (Figure 3). Decreased intercellular adhesion, with resulting increased intercellular clear space, occurred in the dome, mid, and trigone regions. In sections of bladder collected from the mid and trigone regions (but not the dome region), decreased intercellular adhesion with resulting increased intercellular clear space occurred between the superficial umbrella cells and the upper and/or middle intermediate cell layers (bullous formation). This was most often associated with unraveling of the complex interdigitations of lateral and deep plasma membranes of adjacent cells, which led to the presence of prominent microvilli. This cell separation initially involved loss of the normal complex interdigitations of plasma membranes of adjacent cells, with residual attachment remaining at sites of junctional complexes and desmosomes. At sites of bullous formation, apical tight junctions (zona occludens) between superficial cells were generally intact, whereas intermediate junctions (zona adherens) and/or desmosomes (macula adherens) between superficial cells and desmosomes between superficial cells and intermediate cells were generally dissociated (Figure 3). Thus,
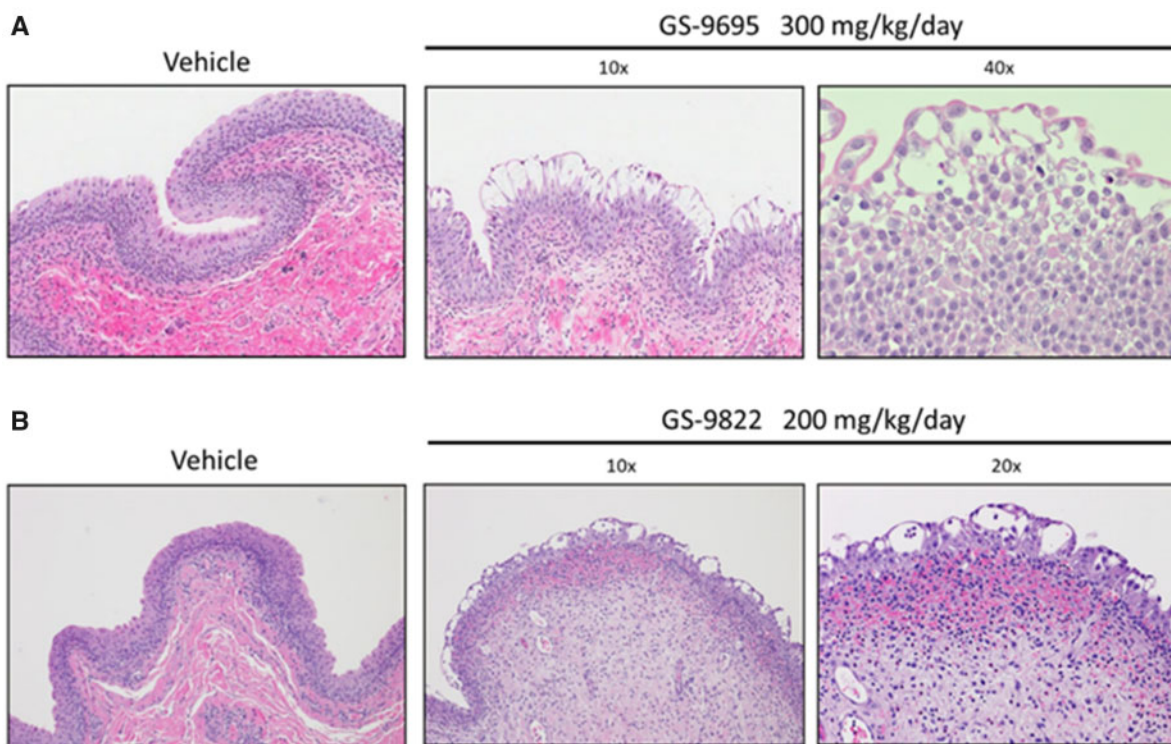
Figure 2. Representative images of cynomolgus monkey bladder urothelium stained with hematoxylin and eosin at 7 days oral gavage treatment with either (A) GS-9695 at 0 (vehicle; 10× magnification) or 300 mg/kg/day at 10× magnification (middle) or 40× magnification (right) or (B) GS-9822 at 0 (vehicle; 10× magnification) or 200 mg/kg/day at 10× magnification (middle) or 20× magnification (right). Transitional cell vacuolation, inflammation and hemorrhage are evident in the treated sections compared with the vehicle only controls.
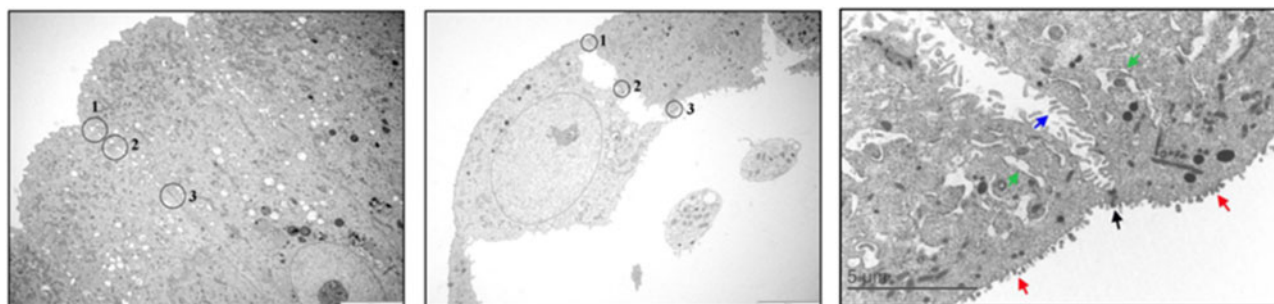
Figure 3. Representative TEM images of cynomolgus monkey urothelium. Left panel (control). Junctional complexes are intact (1 = tight junction or zona occludens; 2 = intermediate junction or zona adherens; 3 = desmosome or macula adherens). Middle panel (urinary bladder from a cynomolgus monkey administered GS-9695 at 300 mg/kg/day). The junctional complexes appear intact on one side of the superficial cell, but there is increased clear space between the adhesion molecules along the lateral surfaces. Note that only the apical tight junction (zona occludens) appears intact on the other side of the cell. The desmosomes along the basal border of the superficial cells are dissociated, and the intermediate cells are no longer in contact with the overlying superficial cells (not in image view). Right panel (urinary bladder from a cynomolgus monkey administered GS-9822 at 200 mg/kg/day). Green arrows (placed in the center of each tissue mass) indicate 2 moderately injured superficial cells with increased cytoplasmic vacuolation. Except for the region of the adluminal junctional complex (black arrow; center bottom of image), there is marked separation of the cells, with the presence of prominent microvilli (blue arrow in the space between cells). Projections from the luminal surface are shorter and plumper than in controls (red arrows on left and right bottom side of image). Left and middle images are at 2650×. Right image is at 12 000×.

superficial cells formed the upper layer, and the separated intermediate cells formed the lower layer of the bullous vacuole. Some rupture of these junctions, especially of desmosomes, was seen with progressing cell injury. Hemidesmosomes between basal urothelial cells and the underlying basal lamina appeared intact. Junctional complexes were occasionally noted in regenerating epithelium.

Secondary Pharmacology
Extensive testing for secondary pharmacological effects potentially mediated by human receptors found that GS-9695 and GS-9822 had inhibitory activity on 6 and 4 targets, respectively. For GS-9695, these targets were platelet-activating factor, glucocorticoid, cannabinoid CB1, histamine H3, melatonin MT1, and prostanoid EP4. For GS-9822, these targets were cholecystokinin CCK, glucocorticoid, adrenergic α2A, and potassium channel (KATP) (see Supplementary Table 5). With the exception of the glucocorticoid receptor, there was no overlap in the off-target pharmacology. This suggested that the observed bladder lesions that were common to both compounds were unlikely to be caused by specific, off-target receptor binding.

Mitochondrial Toxicity

TEM of the urothelium in cynomolgus monkeys indicated mitochondrial swelling of slight to marked severity (Supplementary Figure 1). After 4-h treatment of GS-9695 and GS-9822 in human PC-3 cells, the cellular respiration parameter "spare respiratory capacity" was specifically decreased, before any appreciable effects on ATP level or DNA content were observed (see Supplementary Figures 2A–2C, summarized in Table 2). BI-2244326 had no effect on mitochondrial respiration after 24- or 72-h treatment: a 4-h treatment was not included due to the lack of drug effect after 24-h treatment. GS-9695 and GS-9822 were further tested for their effects on ETC complexes I–V in isolated mitochondrial from mouse liver. GS-9695 and GS-9822 (10 μM) caused 31.5% and 52.4% inhibition on mitochondria complex I activity, respectively. The inhibition was complex I specific and dose dependent (Supplementary Figure 3 and Supplementary Table 6). It should also be noted that these in vitro investigations of mitochondrial toxicity were conducted in human PC3 cells, introducing some limitations in correlating these data to the preclinical findings.

Urinary Concentration and Solubility of GS-9695

Urinalysis in cynomolgus monkeys at day 1 and day 7 of treatment with GS-9695 indicated a mean concentration of GS-9695 in the urine of 5.06 μM (range 0.28–10.84 μM) rising to 16.97 μM (range 1.03–28.15 μM), at day 1 and day 7, respectively (Table 3). Urinalysis in rats at day 1 and day 7 of treatment with GS-9695 indicated a mean concentration of GS-9695 in the urine of 1.32 μM (range 0.55–4.43 μM) dropping to 0.39 μM (range 0.13–0.64 μM), at day 1 and day 7, respectively (Table 3). Although group means varied between rats and cynomolgus monkeys, data points overlapped between species at day 1.

The solubility of GS-9695 in urine was similar between rat and cynomolgus monkey (data not shown). No unexplained solid material, crystalline or otherwise, was detected in any urine samples.

Immunologic Evaluation

In vitro exposure of naïve cynomolgus monkey blood to GS-9695 for 1 h induced the expression of CD16 on monocytes in a concentration-dependent manner (Supplementary Figure 4A) and also increased co-expression of CD16 and CD69 on these cells (Supplementary Figure 4B), suggesting that GS-9695 was capable of increasing the percentage of proinflammatory monocytes as well as state of activation. The addition of LPS alone to the system had minimal effects. In the presence of LPS, GS-9695 was able to induce the expression of CD16 and CD69 double-positive cells but the data were too variable to (relative to LPS and GS-9695 concentration) draw firm conclusions (data not shown). Similarly, the evaluation of expression of CD16 and CD69 on circulating monocytes in animals treated with GS-9695 for 7 days was inconclusive (data not shown). These data suggest that although GS-9695 may be able to induce activated and proinflammatory monocytes in vitro, this is unlikely to be the direct cause of the species-specific effect in the urothelium.

Immunohistochemistry: E-Cadherin and Pan-Cytokeratin

Immunohistochemical analysis of cynomolgus monkey bladder tissue was used to determine if there was any drug-dependent differential expression of key proteins that are required for cell-cell interactions (E-cadherin) or intracellular stability (pan-cytokeratin) (Table 4). The results were similar from both GS-9695 and GS-9822 (data not shown). The membrane stain E-cadherin was present in the urothelium of all animals evaluated (control and dosed groups). In the control animals, there was relatively uniform staining of all layers of the urothelium. In contrast, areas of decreased positive staining were present in almost all dosed animals. These areas predominately involved the superficial and upper intermediate layers of urothelium and were typically centered around regions of vacuolation; lower intermediate and basal urothelial layers stained similar to controls. The regions of vacuolation varied in size, with larger vacuoles distorting the luminal surface and, in some areas, appearing to coalesce and contain cellular debris. Urothelial cells adjacent to these regions often exhibited minimal to no staining for E-cadherin, indicating a loss of intracellular junctions. Cellular debris within the vacuoles rarely exhibited positive staining.

In general, the staining intensity for the cytoplasmic stain pan-cytokeratin was less intense than that of E-cadherin. Pan-cytokeratin was present in the urothelium of all animals evaluated (control and dosed groups) and differences in staining intensity between the control and dosed groups were similar to, though slightly less pronounced and less frequent than, that of E-cadherin. Although decreased staining was typically associated with regions of vacuolation, the cell borders on either side of these regions were still distinct, indicating that the vacuolar spaces were predominately intercellular (ie, between the cells).

Immunohistochemistry: Uroplakins

Immunohistochemical analysis of rat and cynomolgus monkey kidney was carried out to determine expression levels of uroplakins, proteins implicated in the barrier function of mammalian urinary epithelium. There was moderate expression of Uroplakin IIIb-like protein in the nuclei of the cynomolgus monkey tubules and minimal expression in a few nuclei of the glomeruli (Figure 4 and Supplementary Table 7). In contrast, there was no detectable expression of Uroplakin IIIb-like protein in rat kidney tubules and minimal expression in the glomeruli. Some background staining of the rat stroma was also noted.

Surface Activity of GS-9822

An analysis of the physicochemical properties of GS-9822 at a range of pH values was performed to determine if there were any unusual properties that might explain the species-specific bladder toxicity observed in cynomolgus monkeys. The urine is the only unbuffered physiological solution in the body and as such the pH may vary in response to diet. In addition, the normal range is wider in nonhuman primates (normal range 5.5–7.4) and humans (normal range 4.8–7.8) compared with rodents (7.3–8.5) (Hollinger and Derelenko, 2002). The analysis focused on an evaluation of the surface activity of GS-9822 with respect to the pH in solutions with salts added to mimic the typical ionic strength of urine. Two parameters were evaluated: the surface pressure and the ellipsometric phase shift, d(delta). The former is related to the ability of the drug to lower the surface tension of the air/water interface (ie, potential to act as a surfactant) and the latter is a measure of the amount of drug adsorbed to the air/water interface. Figure 5 shows time-resolved measurements of the surface properties of GS-9822 in 3 separate solutions of pH 3, pH 5, and pH 7. (Data from one measurement each are presented here; replicate data can be found in Supplementary Figure 6).

The adsorption process was fastest at pH 7 (Figure 5B), and from d(delta), the amount of GS-9822 adsorbed to the air/water interface reached equilibrium within about 1 min (ie, flattening of the curve in Figure 5B); the gradual increase in the surface pressure with time thereafter (Figure 5A) was probably

Table 2. Effect of GS-9695, GS-9822, and BI-224436 on Mitochondrial Respiration

Compound	Incubation Time (h)	Spare-OCR (µM)	ATP Synthesis (µM)	DNA Concentration (µM)
GS-9695	4	2.33 ± 0.95	11.2 ± 1.0	>50
	24	14 ± 0.14	26 ± 0.2	20 ± 1.8
	72	10 ± 0.24	17 ± 0.9	15 ± 2.5
GS-9822	4	0.76 ± 0.075	6.58 ± 0.19	9.32 ± 1.9
	24	1.08 ± 0.0M	34.1 ± 0.1	36.1 ± 9.8
	72	ND	ND	ND
BI-224436	4	ND	ND	ND
	24	>50	>50	>50
	72	>50	>50	>50
Positive controls	4 (rotenone)	0.0084 ± 0.0066	>0.5	>0.25
	4 (antimycin A)	0.0125 ± 0.0049	>0.5	>0.25
	24 (phenformin)	2.47 ± 0.44	>100	>100
	72 (chloramphenicol)	4.8 ± 1.4	>50	>50

Mitochondrial toxicity was assessed by treating PC-3 cells with increasing concentrations (between 0.2 and 50 µM) of the indicated test agent for 4 h in serum-free culture medium (Kaighn's F12K with 1% penicillin/streptomycin) to assess the potential for acute mitochondrial toxicity, or for 24 or 72 h in culture medium containing 10% fetal bovine serum to assess the potential for chronic mitochondrial toxicity. Rotenone (complex I inhibitor) and antimycin A (complex III inhibitor) were tested between 10 nM and 1 µM while phenformin (complex I inhibitor) was tested between 0.3 and 100 µM. Spare-OCR was normalized with DNA. The values represent the mean ± standard deviation from at least 3 independent measurements. See Supplementary Figures 2A–2C for additional information.
Abbreviations: OCR, oxygen consumption rate, an indication of mitochondrial respiration; ND, not determined.

Table 3. Urinary Concentrations (µM) of GS-9695 in Rats and Cynomolgus Monkeys Administered 300 mg/kg/day for 7 Consecutive Days

Animal	Rat		Monkey	
	Day 1	Day 7	Day 1	Day 7
1	0.758	0.323	0.332	11.65
2	0.685	0.545	4.92	22.06
3	4.425	0.127	10.84	12.67
4	0.553	0.336	0.283	28.15
5	0.568	0.388	8.91	10.31
6	0.931	0.638		
Mean ± SD	1.32 ± 1.53	0.393 ± 0.180	5.06 ± 4.83	16.97 ± 7.80

The data for each day represent the average of the 0–12 and 12–24 h postdose collections.

attributable to minor conformational changes in the packing of the adsorbed monolayer. If the data at pH 7 are taken as a reference, the effects of decreasing pH on the surface characteristics of GS-9822 are pronounced.

At pH 5, the equilibrium surface pressure and hence the surface activity of the drug is similar to that at pH 7 (Figure 5A), but d(delta) as a measure of the amount of drug adsorbed to the air/water interface is almost double (a factor of 1.93: Figure 5B). It follows that the interfacial conformation of GS-9822 changes from a monolayer to a bilayer at the lower pH value. This unusual transition can be explained in terms of a strong association of the drug, which has a somewhat rigid structure (Figure 1C), between bilayer leaflets as a result of its conversion to a zwitterionic character: whereas the carboxylic acid group remains deprotonated (ie, anionic), below pH 7 the piperidine group that is connected to an oxetane group will become protonated (ie, change from neutral to cationic) (Wuitschik et al., 2006, 2010). This result is very interesting in the context that a transition of an adsorbed surfactant monolayer to a bilayer at the air/water interface was only observed for the first time recently (Honnigfort et al., 2020).

At pH 3, the surface activity of the drug is the greatest, demonstrated by the highest magnitude of the surface pressure reached within the measurement time (Figure 5A). However,

the value of d(delta) closely matches that seen at pH 7 (Figure 5B), which indicates a return to an adsorbed monolayer rather than the bilayer seen at pH 5. This transition may be explained again in terms of the drug ionization. Although the piperidine group remains protonated (ie, cationic), below pH 5 the carboxylic acid group will become ionized (ie, change from anionic to neutral) (Smith and March, 2006). Hence, overall the drug transitions from zwitterionic to cationic with a concomitant reduction of the very strong intermolecular association between bilayer leaflets seen at pH 5. Curiously, there is a kink in the data exhibited by both techniques after about 2 min (see red arrows in Figs. 5A and 5B and reproduced in the duplicate experiment; see Supplementary Figure 6). These features point to a surface rearrangement during adsorption where the drug molecules switch conformation as the surface pressure rises resulting in a sudden release of pressure.

DISCUSSION

GS-9695 and GS-9822 were developed as second-generation NCINIs that were structurally distinct from and had improved antiviral potency and resistance profiles compared with BI-224436 (Mitchell et al. 2017). Based on these favorable parameters, GS-9695 progressed into early toxicology testing, followed by GS-9822 when a unique toxicity was observed in cynomolgus monkeys with GS-9695.

Rodent studies showed that at plasma exposure levels within the same range as those predicted to be clinically efficacious, there was little evidence of findings that would preclude clinical development. However, when the drug development program progressed to cynomolgus monkeys, both GS-9695 and GS-9822 caused a dose-dependent vacuolation of the urinary transitional epithelium (urothelium) which lines the inner surface of the renal pelvis, the ureters, and the urinary bladder, where it forms a highly impermeable barrier to ions, solute, and water flux. At higher doses, abnormalities including inflammation and hemorrhage were also seen in the ureter and kidney. In prior nonclinical safety studies with BI-224436, no similar urothelial toxicity was observed but this compound was tested in dogs rather than in nonhuman primates (personal communication).

Table 4. Expression patterns of E-Cadherin and Pan-Cytokeratin Staining in Cynomolgus Monkeys Treated With GS-9695

		Control	Treated
E-cadherin	Superficial and upper intermediate urothelium	+++	+
	Lower intermediate and basal urothelium	+++	+++
Pan-cytokeratin	Superficial and upper intermediate urothelium	++	+
	Lower intermediate and basal urothelium	++	++

Staining intensity: 0, negative; +, mild; ++, moderate; +++, marked.

After confirming that the lesion was reproducible and not the result of artefact from delayed tissue harvest, discussions were initiated to determine the origin of the lesion and its significance for human safety. The first consideration was the target itself since around 40% of drug development failures attributable to safety are associated with target (Cook *et al.*, 2014). However, in this case, the NCINIs specifically target the viral integrase protein and no mammalian homologue is known. Also, BI-224436 progressed successfully into the clinic; development was suspended for reasons unrelated to safety. Regarding the chemistry, GS-9695 and GS-9822 have structurally distinct 2-position substitutions on a shared benzothiazole core (Figure 1) and no direct evidence exists to associate the benzothiazole core with adverse safety concerns (Mitchell *et al.*, 2017). Secondary pharmacology results suggested that the observed bladder lesions were unlikely to be caused by specific, off-target receptor binding.

Given the unique nature of the toxicity observed, an investigative program was initiated to evaluate a possible mode of action (MOA). In the initial investigation with GS-9695, electron microscopy revealed the presence of mitochondria in the superficial cells that were clearly increased in size compared with controls. Mitochondrial toxicity is a common contributor to drug-induced toxicity (Will and Dykens, 2014). Although mitochondrial toxicity was evident with both compounds albeit in PC3 human cells, it is unlikely to cause the species specificity of the urothelial lesion because the histopathology indicated inflammation and disruption of the urothelial morphology rather than cellular necrosis or loss of cellular viability. Furthermore, if mitochondrial dysfunction was the primary MOA, we would have expected to see more systemic and widespread toxicity, especially in tissues such as the heart that are highly susceptible to mitochondrial toxicants.

Exposure to both agents affected only the transitional epithelium in the cynomolgus monkey urinary tract and not in other transitional epithelia, suggesting the possibility of urinary precipitation. Urinary concentration analyses from animals treated with GS-9695 indicated a higher concentration in cynomolgus monkey compared with rat, though the data were quite variable. At appropriate concentrations, transient exposure to an agent targeting the umbrella cells of the urothelium for as few as 15 min may be sufficient to induce damage (LaVelle *et al.*, 2002). It is conceivable then, that transient, high concentrations of GS-9695 may have damaged the urothelium by forming a precipitate. However, this seems unlikely because the data suggest that the drug would have been mostly soluble in the bladder and no unexplained solid material, crystalline or otherwise, was detected in any urine samples.

The bladder of nonhuman primates differs from other mammalian species (such as rodents, dogs, and humans) due to the presence of eosinophilic granules (cytoplasmic inclusions) and mononuclear inflammatory cells normally present in the submucosa and urothelium (Hardisty *et al.*, 2008; Cohen, 2013).

Because histological characterization of the lesion indicated evidence of inflammation, we investigated this as a potential MOA. Although the data suggested that GS-9695 could increase the numbers of CD16+ cells *in vivo*, there was no evidence of monocyte activation, no evidence of a distinctive macrophage infiltrate into the mucosal/submucosal regions, nor any distinctive macrophage association with vacuolation in the urinary bladder, ureter, or kidney (pelvis) urothelium. Therefore, we considered inflammation as an unlikely MOA for the observed findings.

The vacuolation that characterized the lesions was seen extensively in the outer layers of the transitional epithelium, indicative of a sloughing away of layers or sheets of the outermost, viable cells. This suggested that the lesions could be the result of drug-dependent changes in the integrity of cell-cell and/or cell-matrix interactions, associated with the detachment of junctional proteins. The data showed a reduction in E-cadherin (implicated in cell-cell interactions) and in pan-cytokeratin (implicated in intra-cellular stability) in drug-treated cynomolgus monkey tissues for both GS-9695 and GS-9822 treatment. However, in the absence of data for the rat bladder or a plausible reason for the observed species differences in expression and/or modulation of adhesion proteins, interpretation of these findings in the context of a possible MOA is challenging.

The apical surface of mammalian urinary epithelium is covered by numerous scallop-shaped membrane plaques, consisting of 4 different uroplakins. These were of interest because they act as an exceptional barrier to water and toxic materials in urine (Lee, 2011) and are also known to have species specificity in terms of protein structure and expression (Wu *et al.*, 2009). Uroplakin IIIb-like protein has a relatively large cytoplasmic domain which is postulated to play a role in interacting with the cytoskeleton; loss of Uroplakin IIIb-like protein is associated with impairment of the urothelial permeability barrier (Lee, 2011). Although Uroplakin IIIb-like protein was expressed in the kidney of control cynomolgus monkeys, in the absence of any remaining drug-treated cynomolgus monkey tissue, these data were hard to interpret in the context of a possible MOA for the urothelial lesions.

Given the nature of the lesions, particularly the sloughing of intact sheets of viable cells, it seemed plausible that the observed lesions were irritant like and could be attributable to physicochemical changes unique to the bladder. Notably, urine differs markedly from plasma in osmolality and acidity and is not buffered. GS-9822 was investigated to determine its surface activity at a range of pH values relevant to cynomolgus monkey urine. The molecule showed an unusual transition from a monolayer to a bilayer at the air/water interface at pH 5, attributed to the strong association between drug molecules in adjacent bilayer leaflets resulting from a zwitterionic characteristic that exists over only a narrow range of pH values (pH 4–7). This surface rearrangement during drug adsorption would be
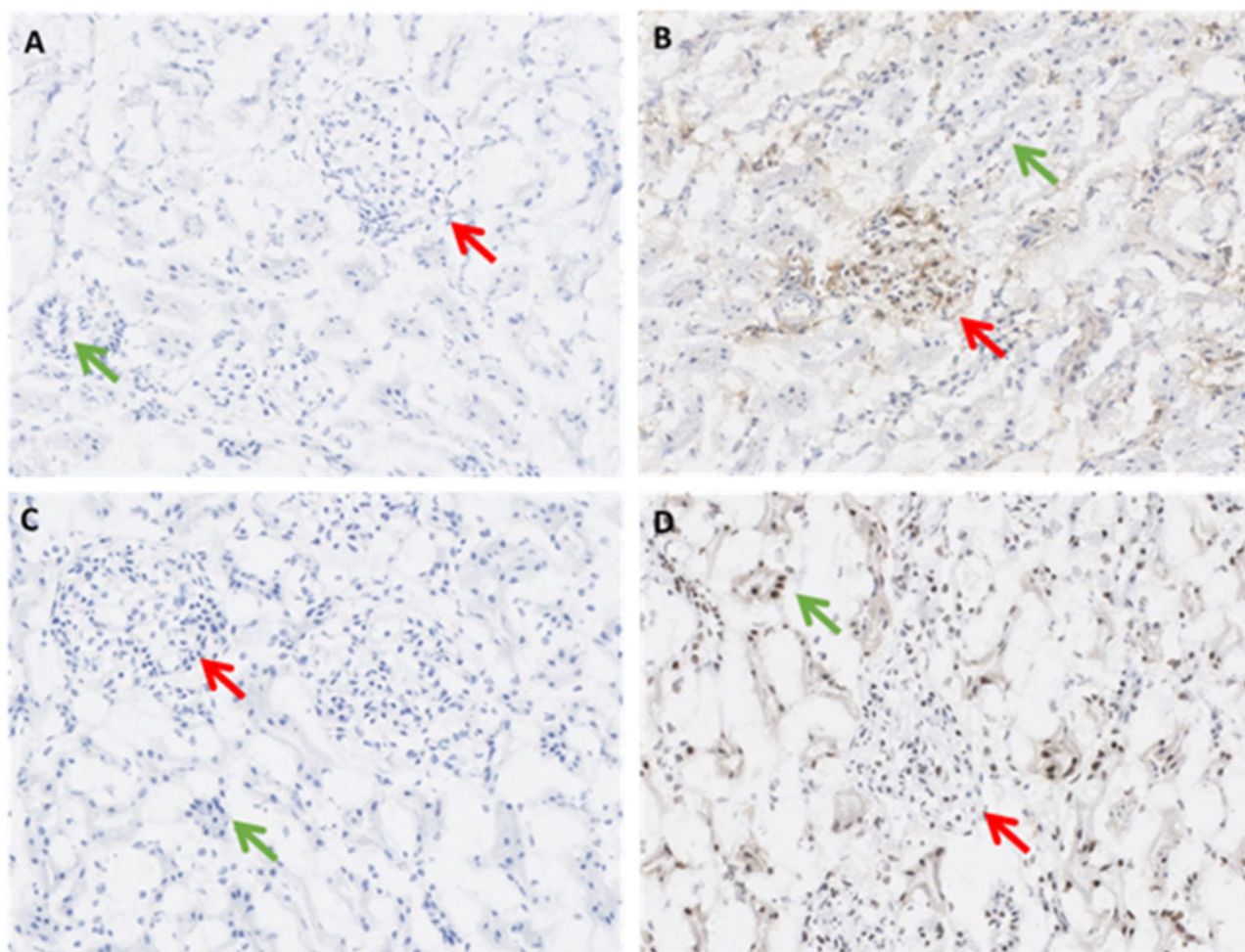
Figure 4. Uroplakin IIIb expression in the rat and cynomolgus monkey kidney. A, rat—negative control, B, rat—UPK3BL staining, C, cynomolgus monkey—negative control, and D, cynomolgus monkey—UPK3BL staining. Images taken at 20× magnification. (Tubules and glomeruli are indicated with arrows.)
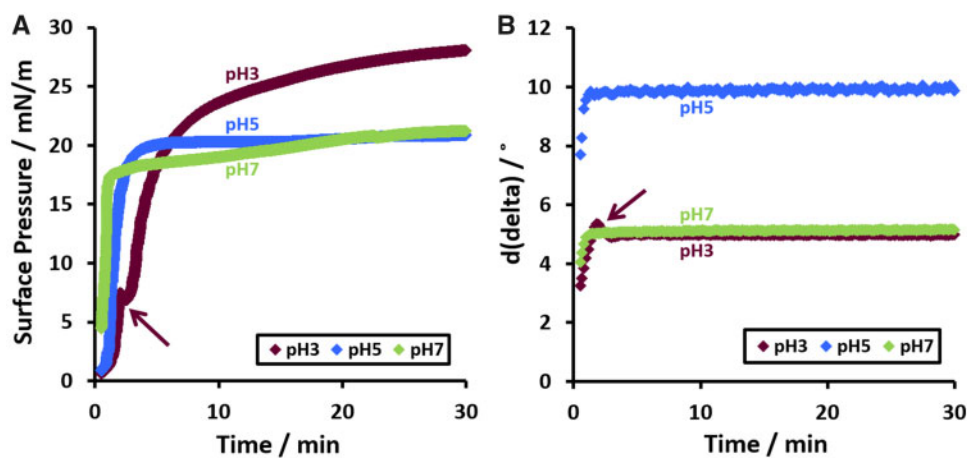

Figure 5. Time-resolved measurements of (A) the surface pressure and (B) ellipsometric phase shift at the air/water interface for solutions of 20 μM GS-9822 in 0.1 M NaCl/0.1 M KCl with respect to the solution pH; aspiration was used to set the zero time point. The former (A) is related to the ability of the drug to lower the surface tension of the air/water interface and the latter (B) is a measure of the amount of adsorbed drug.

expected to be highly disruptive to the integrity of the cell membrane. Additionally, this transition would not be expected to occur in rat urine due to the pH differences, though it is plausible that it may occur in humans. A transition of an adsorbed surfactant from monolayer to a bilayer at the air/water interface is a newly discovered phenomenon, first reported as an unexpected finding recently (Honnigfort et al., 2020). One approach might be to test biological plausibility by assessing the impact

of the drug on cultured cells at pH 5 or 6. However, anything more than a slight reduction in pH causes cells to lyse making it impractical to test this hypothesis *in vitro* in any meaningful way.

GS-9822 and GS-9695 have fairly rigid or inflexible chemical structures as a result of their aromatic groups, which restrict the degree to which they can change conformation (Figure 1). Furthermore, due to the zwitterionic nature of the molecule, the groups at either end have different potentials for ionization depending on the pH. Importantly, BI-224436 is markedly different in the key properties implicated in the detergent-like activities of GS-9822 and GS-9695. Specifically, there is neither a piperidine nor a piperazine group in BI-224436 and so its carboxylic group will simply transition the molecule from neutral to cationic (never zwitterionic) with decreasing pH. Hence it follows that the exotic surface behavior observed with GS-9822 would be absent in BI-224436.

In summary, GS-9695 and GS-9822 are next-generation NCINIs with significantly improved potency against HIV compared with BI-224436 (Mitchell *et al.*, 2017) but were halted in development due to a bladder lesion in the monkey. Investigations of potential MOAs such as secondary pharmacology, mitochondrial respiration, immune activation, or interference with the expression of function of cellular adhesion molecules were all inconclusive. Noting that the lesions were restricted to the urothelium in cynomolgus monkeys, we postulated that the changes could be attributable to physicochemical changes within the bladder, especially at low or changing pH. Studies of surface pressure pointed to a surface rearrangement during the course of drug adsorption where the drug molecules switch conformation, a transformation expected to be highly disruptive to the integrity of the cell membrane. Evidence also suggested a higher urinary concentration of drug in the cynomolgus monkey compared with the rat. A possible avenue for future work could be a structural characterization of GS-9822 using neutron reflectometry, which has been shown to be powerful in resolving structural transitions of drugs and their time-resolved interactions with model biological membranes (Campbell, 2018; Matyszewska *et al.*, 2021).

In conclusion, although there are some gaps in the data, they provide useful insights to guide current or future clinical development of NCINIs, related compounds, and those with zwitterionic characteristics. Specifically, the structure-toxicity relationship inferred from the data on GS-9822/9695 compared with BI-224436 suggest that novel NCINIs can be developed providing modeling is employed to ensure the rigid zwitterionic characteristics described here can be avoided.

SUPPLEMENTARY DATA

Supplementary data are available at *Toxicological Sciences* online.

ACKNOWLEDGMENTS

DECLARATION OF CONFLICTING INTERESTS

REFERENCES

Angus-Smyth, A., Campbell, R. A., and Bain, C. D. (2012). Dynamic adsorption of weakly interacting polymer/surfactant mixtures at the air/water interface. *Langmuir* **28**, 12479–12492.

Benit, P., Goncalves, S., Philippe Dassa, E., Briere, J. J., Martin, G., and Rustin, P. (2006). Three spectrophotometric assays for the measurement of the five respiratory chain complexes in minuscule biological samples. *Clin. Chim. Acta* **374**, 81–86.

Buron, N., Porceddu, M., Brabant, M., Desgue, D., Racoeur, C., Lassalle, M., Pechoux, C., Rustin, P., Jacotot, E., and Borgne-Sanchez, A. (2010). Use of human cancer cell lines mitochondria to explore the mechanisms of BH3 peptides and ABT-737-induced mitochondrial membrane permeabilization. *PLoS One* **5**, e9924.

Campbell, R. A. (2018). Recent advances in resolving kinetic and dynamic processes at the air/water interface using specular neutron reflectometry. *Curr. Opin. Colloid Interface Sci.* **37**, 49–60.

Cohen, S.M. (2013). Lower urinary tract. In *Haschek and Rousseaux's Handbook of Toxicologic Pathology*, 3rd ed. (W. M. Haschek, C. G. Rousseaux, M. A. Wallig, B. Bolon, and R. OchoaI, Eds.), Vol. **3**, Chapter 48, p. 1775ff. Elsevier Science Publishing Co Inc, Academic Press Inc, Amsterdam, Netherlands.

Cook, D., Brown, D., Alexander, R., March, R., Morgan, P., Satterthwaite, G., and Pangalos, M. N. (2014). Lessons learned from the fate of AstraZeneca's drug pipeline: A five-dimensional framework. *Nat. Rev. Drug Discov.* **13**, 419–431.

de Feijter, J. A., Benjamins, J., and Veer, F. A. (1978). Ellipsometry as a tool to study the adsorption behavior of synthetic and biopolymers at the air-water interface. *Biopolymers* **17**, 1759–1772.

Dranka, B. P., Benavides, G. A., Diers, A. R., Giordano, S., Zelickson, B. R., Reily, C., Zou, L., Chatham, J. C., Hill, B. G., Zhang, J., *et al.* (2011). Assessing bioenergetic function in response to oxidative stress by metabolic profiling. *Free Radic. Biol. Med.* **51**, 1621–1635.

Ducharme, D., Max, J. J., Salesse, C., and Leblanc, R. M. (1990). Ellipsometric study of the physical states of phosphatidylcholines at the air-water interface. *J. Phys. Chem.* **94**, 1925–1932.

Engelman, A., and Cherepanov, P. (2008). The lentiviral integrase binding protein LEDGF/p75 and HIV-1 replication. *PLoS Pathog* **4**, e1000046.

Fader, L. D., Malenfant, E., Parisien, M., Carson, R., Bilodeau, F., Landry, S., Pesant, M., Brochu, C., Morin, D. S., Chabot, C., *et al.* (2014). Discovery of BI 224436, a noncatalytic site integrase inhibitor (NCINI) of HIV-1. *ACS Med. Chem. Lett.* **5**, 422–427.

Feng, J. Y., Xu, Y., Barauskas, O., Perry, J. K., Ahmadyar, S., Stepan, G., Yu, H., Babusis, D., Park, Y., McCutcheon, K., *et al.*

(2016). Role of mitochondrial RNA polymerase in the toxicity of nucleotide inhibitors of hepatitis C virus. *Antimicrob. Agents Chemother*. **60**, 806–817.

Hardisty, J. F., Anderson, D. C., Brodie, S., Cline, J. M., Hahn, F. F., Kolenda-Roberts, H., Lele, S. M., and Lowenstine, L. J. (2008). Histopathology of the urinary bladders of cynomolgous monkeys treated with PPAR agonists. *Toxicol. Pathol*. **36**, 769–776.

Hollinger, M. A., and Derelenko, M. J., eds. (2002). Miscellaneous information of toxicological significance. In *Handbook of Toxicology*, 2nd ed., Chapter 33, p. 1235ff. CRC Press, London, UK.

Honnigfort, C., Campbell, R. A., Droste, J., Gutfreund, P., Hansen, M. R., Ravoo, B. J., and Braunschweig, B. (2020). Unexpected monolayer-to-bilayer transition of arylazopyrazole surfactants facilitates superior photo-control of fluid interfaces and colloids. *Chem. Sci*. **11**, 2085–2092.

Jurado, K. A., Wang, H., Slaughter, A., Feng, L., Kessl, J. J., Koh, Y., Wang, W., Ballandras-Colas, A., Patel, P., Fuchs, J., *et al*. (2013). Allosteric integrase inhibitor potency is determined through the inhibition of HIV-1 particle maturation. *Proc. Natl. Acad. Sci. U.S.A*. **110**, 8690–8695.

Kessl, J. J., Jena, N., Koh, Y., Taskent-Sezgin, H., Slaughter, A., Feng, L., de Silva, S., Wu, L., Le Grice, S., Engelman, A., *et al*. (2012). Multimode, cooperative mechanism of action of allosteric HIV-1 integrase inhibitors. *J. Biol. Chem*. **287**, 16801–16811.

LaVelle, B., Meyers, S., Ramage, R., Bastacky, S., Doty, D., Apodaca, G., and Zeidel, M. L. (2002). Bladder permeability barrier: Recovery from selective injury of surface epithelial cells. *Am. J. Physiol. Renal Physiol*. **283**, F242–F253.

Lecoeur, H., Langonne, A., Baux, L., Rebouillat, D., Rustin, P., Prevost, M. C., Brenner, C., Edelman, L., and Jacotot, E. (2004). Real-time flow cytometry analysis of permeability transition in isolated mitochondria. *Exp. Cell Res*. **294**, 106–117.

Lee, G. (2011). Uroplakins in the lower urinary tract. *Int. Neurourol. J*. **15**, 4–12.

Llano, M., Saenz, D. T., Meehan, A., Wongthida, P., Peretz, M., Walker, W. H., Teo, W., and Poeschla, E. M. (2006). An essential role for LEDGF/p75 in HIV integration. *Science* **314**, 461–464.

Marshall, H. M., Ronen, K., Berry, C., Llano, M., Sutherland, H., Saenz, D., Bickmore, W., Poeschla, E., and Bushman, F. D. (2007). Role of PSIP 1/LEDGF/p75 in lentiviral infectivity and integration targeting. *PLoS One* **2**, e1340.

Matyszewska, D., Nazaruk, E., and Campbell, R. A. (2021). Interactions of anticancer drugs doxorubicin and idarubicin with lipid monolayers: New insight into the composition, structure and morphology. *J. Coll. Interface Sci*. **581**, 403–406.

Mitchell, M., Balakrishnan, M., Brizgys, G., Cai, R., Lansdon, E., Mulato, A., Osier, M., wang, J., Yu, H., and Sakowicz, R. (2017). Novel non-catalytic site integrase inhibitor with improved resistance profile. *Conference on Retroviruses and Opportunistic Infections (CROI)*, February 13–16, 2017, Seattle, Washington. Abstract 343. Available at: http://www.croiwebcasts.org/p/2017croi/croi33637. Accessed Jue 22, 2021.

Park, H.-K., Cho, J.-W., Lee, B.-S., Park, H., Han, J.-S., Yang, M.-J., Wan-Jung, I., Park, W.-J., Kim, D.-Y., Han, W.-J., *et al*. (2016). Reference values of clinical pathology parameters in cynomolgus monkeys (*Macaca fascicularis*) used in preclinical studies. *Lab. Anim. Res*. **32**, 79–86.

Poeschla, E. M. (2008). Integrase, LEDGF/p75 and HIV replication. *Cell Mol. Life Sci*. **65**, 1403–1424.

Pommier, Y., Johnson, A. A., and Marchand, C. (2005). Integrase inhibitors to treat HIV/AIDS. *Nat. Rev. Drug Discov*. **4**, 236–248.

Rustin, P., Chretien, D., Bourgeron, T., Gerard, B., Rotig, A., Saudubray, J. M., and Munnich, A. (1994). Biochemical and molecular investigations in respiratory chain deficiencies. *Clin. Chim. Acta* **228**, 35–51.

Schrijvers, R., De Rijck, J., Demeulemeester, J., Adachi, N., Vets, S., Ronen, K., Christ, F., Bushman, F., Debyser, Z., and Gijsbers, R. (2012). LEDGF/p75-independent HIV-1 replication demonstrates a role for HRP-2 and remains sensitive to inhibition by LEDGINs. *PLoS Pathog*. **8**, e1002558.

Shun, M.-C., Raghavendra, N. K., Vandegraaff, N., Daigle, J. E., Hughes, S., Kellam, P., Cherepanov, P., and Engelman, A. (2007). LEDGF/p75 functions downstream from preintegration complex formation to effect gene-specific HIV-1 integration. *Genes Dev*. **21**, 1767–1778.

Smith, M. B., and March, J. (2006). *March's Advanced Organic Chemistry*. John Wiley & Sons, Inc., Hoboken, NJ.

Tsiang, M., Jones, G. S., Niedziela-Majka, A., Kan, E., Lansdon, E. B., Huang, W., Hung, M., Samuel, D., Novikov, N., Xu, Y., *et al*. (2012). New class of HIV-1 integrase (IN) inhibitors with a dual mode of action. *J. Biol. Chem*. **287**, 21189–21203.

Tummino, A., Toscano, J., Sebastiani, F., Noskov, B. A., Varga, I., and Campbell, R. A. (2018). Effects of aggregate charge and subphase ionic strength on the properties of spread polyelectrolyte/surfactant films at the air/water interface under static and dynamic conditions. *Langmuir* **34**, 2312–2323.

Vandekerckhove, L., Christ, F., Van Maele, B., De Rijck, J., Gijsbers, R., Van den Haute, C., Witvrouw, M., and Debyser, Z. (2006). Transient and stable knockdown of the integrase cofactor LEDGF/p75 reveals its role in the replication cycle of human immunodeficiency virus. *J. Virol*. **80**, 1886–1896.

Will, Y., and Dykens, J. (2014). Mitochondrial toxicity assessment in industry - A decade of technology development and insight. *Exp. Opin. Drug Metab. Toxicol*. **10**, 1061–1067.

Wu, X. R., Kong, X. P., Pellicer, A., Kreibich, G., and Sun, T. T. (2009). Uroplakins in urothelial biology, function, and disease. *Kidney Int*. **75**, 1153–1165.

Wuitschik, G., Carreira, E. M., Wagner, Brn., Fischer, H., Parrilla, I., Schuler, F., Rogers-Evans, M., and Müller, K. (2010). Oxetanes in drug discovery: Structural and synthetic insights. *J. Med. Chem*. **53**, 3227–3246.

Wuitschik, G., Rogers-Evans, M., Müller, K., Fischer, H., Wagner, B., Schuler, F., Polonchuk, L., and Carreira, E. M. (2006). Oxetanes as promising modules in drug discovery. *Angew. Chem*. **118**, 7900–7903.